

Potential impact of noise correlation in next-generation gravitational wave detectors

Isaac C. F. Wong^{1,2,*} Peter T. H. Pang^{3,4} Milan Wils^{5,2} Francesco
Cireddu^{5,6,7,2} Walter Del Pozzo^{6,7} and Tjonnie G. F. Li^{5,1,2}

¹*KU Leuven, Department of Electrical Engineering (ESAT), STADIUS Center for Dynamical Systems,
Signal Processing and Data Analytics, Kasteelpark Arenberg 10, 3001 Leuven, Belgium*

²*Leuven Gravity Institute, KU Leuven, Celestijnenlaan 200D box 2415, 3001 Leuven, Belgium*

³*Institute for Gravitational and Subatomic Physics (GRASP),
Utrecht University, Princetonplein 1, 3584 CC Utrecht, The Netherlands*

⁴*Nikhef, Science Park 105, 1098 XG Amsterdam, The Netherlands*

⁵*Institute for Theoretical Physics, KU Leuven, Celestijnenlaan 200D, B-3001 Leuven, Belgium*

⁶*Dipartimento di Fisica “E. Fermi”, Università di Pisa, I-56127 Pisa, Italy*

⁷*INFN, Sezione di Pisa, I-56127 Pisa, Italy*

(Dated: February 25, 2025)

Building upon the statistical formulation for parameter estimation in the presence of correlated noise proposed by Cireddu *et al.*, we present the initial study to incorporate the effects of correlated noise into the analyses of various detector designs’ performance. We consider a two-L-shaped-detector configuration located in Europe and compare the expectation of parameter estimation of gravitational wave transients between noncollocated and hypothetical collocated configurations. In our study, we posit the existence of low-frequency correlated noise within the 5–10 Hz range for the collocated detector configuration, with a varying degree of correlation. In this specific detector setup, our observations indicate an enhancement in the precision of intrinsic parameter measurements as the degree of correlation increases. This trend suggests that higher degrees of noise correlation may beneficially influence the accuracy of parameter estimation. In particular, when the noise is highly correlated, the uncertainty on chirp mass decreases by up to 30%. The absence of an inter-European baseline does hinder the estimation of the extrinsic parameters. However, given a realistic global network with the additional detector located in the United States, the uncertainty of extrinsic parameters is significantly reduced. This reduction is further amplified as the degree of noise correlation increases. When the degree of noise correlation exceeds a certain level, the collocated configuration outperforms the noncollocated configuration. For instance, when the degree of correlation is high, the collocated configuration decreases the 90% credible area of sky location by up to 10% compared to the noncollocated configuration. We conclude that the impact of noise correlation is not trivial and can potentially alter both the quantitative and qualitative outcomes in detector performance. We therefore recommend the inclusion of noise correlation for a comprehensive assessment of the design of third-generation gravitational wave detectors.

I. INTRODUCTION

Since the first detection of gravitational waves (GWs) in 2015 [1], almost a hundred GW signals from binary mergers have been detected [2]. Such detections have significantly impacted various aspects of astronomy and fundamental physics [3–5]. The next-generation GW detectors promise to unlock mysteries in astrophysics, fundamental physics, and cosmology [6–9]. One such proposal is the Einstein Telescope (ET) [10], a third-generation ground-based GW detector.

One of the proposals for the ET consists of a collocated detector network. Such a setting gives rise to a novel challenge, namely, correlated detector noise. Because of the proximity of the collocated detectors [11], the noise in each of the detectors is expected to have a non-negligible correlation. The correlation is likely coming from seismic perturbations, Newtonian noise [12, 13], and magnetic fluctuation [14, 15]. While the literature

recognizes the profound implications of correlated noise, existing research predominantly addresses its influence on the search of isotropic stochastic GW background [12–15]. A recent study [13] reports that the seismic correlations are significant over several hundreds of meters to a few kilometers in the frequency range 0.01–40 Hz. Notably, the impact of correlated noise on GW transients has not been factored into the most recent extensive evaluation of various ET designs [7]. This omission highlights an important gap in our understanding and underscores the necessity for comprehensive studies that integrate the effects of correlated noise into the evaluation of detector configurations, thereby ensuring more accurate and robust design comparisons for the ET.

Conventional GW parameter estimation [16, 17] assumes uncorrelated detector noise. There have been studies on the Laser Interferometer Space Antenna (LISA) that include noise correlation in their analyses [18, 19]. These works acknowledge the presence of noise correlation and make specific assumptions about it. However, the impact of noise correlation on parameter estimation was not the primary focus of these studies. Recent work by Cireddu *et al.* [20] introduces a statistical for-

* chunfung.wong@kuleuven.be

mulation to account for correlated noise which is similar to the approach used in LISA analyses. This work lays a foundation for investigating the impact of noise correlation on parameter estimation, which is highly relevant for studies like ours that aim to explore these effects in more detail.

In this manuscript, we present a statistical framework to integrate the effects of correlated noise in the evaluation of different GW detector designs. Our approach involves numerical analyses aimed at understanding how correlated noise influences the accuracy of parameter estimation for GW transients. A colocated two-L-shaped configuration is often used as a proxy for a triangular configuration in the literature. However, in the presence of correlated noise, this is no longer generally the case. Nevertheless, to isolate the effects of correlated noise from benefits specifically due to detector geometry, such as null stream, our study focus exclusively on two L-shaped detectors under two distinct scenarios: one in which the detectors are colocated and another where they are noncollocated. We assess the impact on parameter estimation uncertainty through Fisher information matrix (FIM) analysis to make a global assessment of a population of sources. Remarkably, our findings reveal that, within the particular detector configuration examined, the presence of noise correlation leads to enhanced precision in parameter estimation compared to a comparable, yet noncollocated, detector network.

Hence, our research challenges the prevailing notion that noise correlation invariably compromises the scientific output of a detector network. Instead, it furnishes compelling evidence of the nontrivial impacts of noise correlation. This insight not only broadens our understanding of the interplay between detector configuration

and noise characteristics, but also underscores the necessity of reevaluating design strategies in light of these findings.

II. REVIEW OF CORRELATED NOISE STATISTICS

In this section, we review the likelihood formulation in the presence of correlated noise presented in Ref. [20] in the context of two detectors.

The data of the two detectors are denoted as the time series \mathbf{x}_j , where $j = 1, 2$. These time series are sampled at regular intervals of Δt . We express the time series of multiple detectors as a matrix \mathbf{X} , where each row j corresponds to the time series of the j th detector. To compactly represent the spatial-temporal correlations in the noise data, we vectorize the matrix \mathbf{X} into a single vector \mathbf{x} as follows:

$$\mathbf{x} := \text{vec}(\mathbf{X}^T) = \begin{bmatrix} \mathbf{x}_1 \\ \mathbf{x}_2 \end{bmatrix}. \quad (1)$$

$\tilde{\mathbf{x}}$ is understood to be the vectorization of the Fourier transform of the individual time series as follows:

$$\tilde{\mathbf{x}} = \begin{bmatrix} \tilde{\mathbf{x}}_1 \\ \tilde{\mathbf{x}}_2 \end{bmatrix}. \quad (2)$$

The strain data are denoted as \mathbf{d} . The GW signal is denoted as $\mathbf{s}(\boldsymbol{\theta})$ given the source parameters $\boldsymbol{\theta} \in \mathbb{R}^D$.

Assuming the noise follows the stationary Gaussian distribution, the likelihood function can be shown to be

$$p(\mathbf{d}|\boldsymbol{\theta}) = \frac{1}{\det(\pi \mathbf{S}_n / (2\Delta f))} \exp \left(-\frac{1}{2} \langle \mathbf{d} - \mathbf{s}(\boldsymbol{\theta}), \mathbf{d} - \mathbf{s}(\boldsymbol{\theta}) \rangle \right), \quad (3)$$

where \mathbf{S}_n is the spectral matrix defined as follows:

$$\mathbf{S}_n = \begin{bmatrix} \mathbf{S}_n^{11} & \mathbf{S}_n^{12} \\ \mathbf{S}_n^{21} & \mathbf{S}_n^{22} \end{bmatrix}, \quad (4)$$

where

$$\mathbf{S}_n^{\ell m}[j, k] = 2\Delta f \delta_{jk} \mathbb{E}[\tilde{n}_\ell[j] \tilde{n}_m^*[k]] \quad (5)$$

with δ_{jk} being the Kronecker delta function. $\mathbf{S}_n^{\ell\ell}$ is the one-sided power spectral density (PSD) of the noise in the ℓ th detector, and $\mathbf{S}_n^{\ell m}$ is the cross spectral density (CSD) of the noise in the ℓ th and the m th detectors. One should be reminded that our definition of CSD differs from the conventional definition by a complex conjugate. $\langle \mathbf{x}, \mathbf{y} \rangle$ is

the generalized noise-weighted inner product defined as

$$\langle \mathbf{x}, \mathbf{y} \rangle = 4\Delta f \text{Re} \left(\sum_{\ell, m=1}^2 \sum_{k=k_{\text{low}}}^{k_{\text{high}}} (\mathbf{S}_n^{-1})^{\ell m}[k, k] \tilde{x}_\ell[k] \tilde{y}_m[k] \right), \quad (6)$$

where Δf is the frequency resolution, and the inner product evaluated between $f_{\text{low}} = \Delta f k_{\text{low}}$ and $f_{\text{high}} = \Delta f k_{\text{high}}$, where $k_{\text{low}} > 0$ and $k_{\text{high}} < \lfloor N/2 \rfloor - 1$, where N is the length of the time series.

III. REDUCED SPREAD OF THE NOISE DISTRIBUTION IN THE PRESENCE OF CORRELATED NOISE

While the noise model in Eq. (3) accounts for the spatial-temporal correlation in the strain data of the ET, the impact of such correlation on parameter estimation has not yet been studied. Two scenarios are considered to detail the effects of correlated noise: (i) Detectors are collocated, experiencing correlated noise, e.g., seismic noise. The corresponding noise spectral matrix is denoted as

$$\mathbf{S}_n^{\text{corr}} = \begin{bmatrix} \mathbf{S}_n^{11} & \mathbf{S}_n^{12} \\ \mathbf{S}_n^{21} & \mathbf{S}_n^{22} \end{bmatrix}. \quad (7)$$

(ii) Detectors are noncollocated, with the extent of separation not leading to a complete alteration in environmental noise sources. Nevertheless, they still have a similar noise properties, leading to the same noise covariance matrix as scenario (i), except for the vanishing nondiagonal elements. The corresponding noise covariance matrix is given by

$$\mathbf{S}_n^{\text{uncorr}} = \begin{bmatrix} \mathbf{S}_n^{11} & \mathbf{0} \\ \mathbf{0} & \mathbf{S}_n^{22} \end{bmatrix}. \quad (8)$$

At this point, we can already obtain insights into the impact of correlated noise on the measurement process. The spread of the Gaussian distribution is proportional to the square root of the determinant of the covariance or

spectral matrix. From Fischer's inequality [21], we can deduce the following inequality:

$$\sqrt{\det \mathbf{S}_n^{\text{corr}}} \leq \sqrt{\det \mathbf{S}_n^{\text{uncorr}}}, \quad (9)$$

from which one can conclude that the presence of correlated noise [i.e., nonzero off-diagonal blocks in Eq. (7)] actually reduces of the spread of the likelihood function in Eq. (3). The propagation of the reduced spread to the precision of parameter estimation is, however, not trivial. We emphasize that one cannot immediately conclude from the reduced spread that it would result in a more precise parameter estimation, since a more careful analysis would reveal that the specific structure of the signal gradient is another important factor. It is, however, tempting to speculate that the impact of noise correlation is not always negative.

IV. IMPACT OF CORRELATED NOISE ON PARAMETER ESTIMATION

To compare the performance, we assess how the uncertainty of parameter estimation changes between the two detector configurations when observing the same source. This comparison is characterized by the ratio of the square root of the determinant of the covariance matrix of the posterior distributions, averaged over noise realizations:

$$r_{\text{uncorr}}^{\text{corr}} := \frac{\mathbb{E}_{\mathbf{d}^{\text{corr}}|\boldsymbol{\theta}_{\text{true}}} \left[\sqrt{\det(\boldsymbol{\Sigma}_{\boldsymbol{\theta}}|\mathbf{S}_n^{\text{corr}})} \right]}{\mathbb{E}_{\mathbf{d}^{\text{uncorr}}|\boldsymbol{\theta}_{\text{true}}} \left[\sqrt{\det(\boldsymbol{\Sigma}_{\boldsymbol{\theta}}|\mathbf{S}_n^{\text{uncorr}})} \right]} = \frac{\int \sqrt{\det(\boldsymbol{\Sigma}_{\boldsymbol{\theta}}|\mathbf{S}_n^{\text{corr}})} p(\mathbf{d}^{\text{corr}}|\boldsymbol{\theta}_{\text{true}}, \mathbf{S}_n^{\text{corr}}) d\mathbf{d}^{\text{corr}}}{\int \sqrt{\det(\boldsymbol{\Sigma}_{\boldsymbol{\theta}}|\mathbf{S}_n^{\text{uncorr}})} p(\mathbf{d}^{\text{uncorr}}|\boldsymbol{\theta}_{\text{true}}, \mathbf{S}_n^{\text{uncorr}}) d\mathbf{d}^{\text{uncorr}}} \quad (10)$$

where $\boldsymbol{\Sigma}_{\boldsymbol{\theta}}|\mathbf{S}_n^{\text{corr}/\text{uncorr}}$ is the posterior covariance of the model parameters $\boldsymbol{\theta}$ given a noise realization with the noise spectral matrix $\mathbf{S}_n^{\text{corr}/\text{uncorr}}$, and $\boldsymbol{\theta}_{\text{true}}$ is the true parameters.

Evaluating the quantity $r_{\text{uncorr}}^{\text{corr}}$ is challenging for general setups. Instead, we turn to the FIM analysis. The inverse of the FIM is known to characterize the covariance of the posterior distribution in the high signal-to-noise ratio (SNR) limit [22]. For a deterministic signal $\mathbf{s}(\boldsymbol{\theta})$, the FIM is given by

$$\mathcal{I}_{jk}^{\text{corr}/\text{uncorr}}(\boldsymbol{\theta}) = \langle \partial_{\theta_j} \mathbf{s}(\boldsymbol{\theta}), \partial_{\theta_k} \mathbf{s}(\boldsymbol{\theta}) \rangle|_{\mathbf{S}_n=\mathbf{S}_n^{\text{corr}/\text{uncorr}}} \quad (11)$$

where $\partial_{\theta_j} \mathbf{s}(\boldsymbol{\theta})$ is the derivative of the signal with respect to the j th model parameter. In the high SNR limit, the ratio $r_{\text{uncorr}}^{\text{corr}}$ is then reduced to:

$$\hat{r}_{\text{uncorr}}^{\text{corr}} = \frac{1/\sqrt{\det(\mathcal{I}^{\text{corr}}(\boldsymbol{\theta}_{\text{true}}))}}{1/\sqrt{\det(\mathcal{I}^{\text{uncorr}}(\boldsymbol{\theta}_{\text{true}}))}}, \quad (12)$$

$\hat{r}_{\text{uncorr}}^{\text{corr}} < 1$ is indicating an improvement in parameter estimation precision, and vice versa. The mathematical properties of $\hat{r}_{\text{uncorr}}^{\text{corr}}$ are further studied in Appendix A.

A. Simulation

We consider two scenarios. In the first one, we simulate two L-shaped detectors located in Europe (EU) with a 45° relative offset and identical PSDs, the ET-D sensitivity $\mathbf{S}_n^{\text{ET-D}}$ [23]. Within this scenario, we compare two configurations: (i) the two detectors are noncollocated, with one placed at Limburg and one at Sardinia, featuring uncorrelated noise, denoted by the spectral matrix $\mathbf{S}_n^{\text{uncorr}}$, while for ii) the two detectors are collocated at Limburg, featuring correlated noise, represented by the spectral matrix $\mathbf{S}_n^{\text{corr}}$. The orientation, elevation, and arm length are the same across the two setups. The locations and orientations of Ref. [24] are used for the EU

detectors.

In the second scenario, we consider a simulated global network with an L-shaped detector located at Hanford, referred as the US detector in the text, with the 40 km sensitivity of the Cosmic Explorer $S_n^{\text{CE-40km}}$ [25–27].

In the simulation, we use the frequency cutoff to be [5, 1024) Hz. In the absence of a faithful correlated (seismic) noise model, we assume the noise components under 10 Hz are correlated with a correlation coefficient of α . Consequently, the CSD for the EU detectors is taken to be $\alpha S_n^{\text{ET-D}}(f)$ for $f \leq 10$ Hz and 0 otherwise.

It should be noted that the CSD, which represent the cross covariance of noise between different detectors, is generally complex. This complexity arises from time delays of noise disturbances across detectors. For simplicity, our simulation assumes that the correlation coefficient α is real. This assumption helps in focusing on the impact of varying noise correlation levels on parameter estimation.

Therefore, the spectral matrices for a sole EU network are given by

$$\begin{aligned} \mathbf{S}_n^{\text{uncorr}} &= \begin{bmatrix} S_n^{\text{ET-D}} & \mathbf{0} \\ \mathbf{0} & S_n^{\text{ET-D}} \end{bmatrix}, \\ \mathbf{S}_n^{\text{corr}} &= \begin{bmatrix} S_n^{\text{ET-D}} & \alpha S_n^{\text{ET-D}} \\ \alpha S_n^{\text{ET-D}} & S_n^{\text{ET-D}} \end{bmatrix}, \end{aligned} \quad (13)$$

and, for a global network with the inclusion of a US detector, the matrices are given by

$$\begin{aligned} \mathbf{S}_n^{\text{uncorr}} &= \begin{bmatrix} S_n^{\text{ET-D}} & \mathbf{0} & \mathbf{0} \\ \mathbf{0} & S_n^{\text{ET-D}} & \mathbf{0} \\ \mathbf{0} & \mathbf{0} & S_n^{\text{CE-40km}} \end{bmatrix}, \\ \mathbf{S}_n^{\text{corr}} &= \begin{bmatrix} S_n^{\text{ET-D}} & \alpha S_n^{\text{ET-D}} & \mathbf{0} \\ \alpha S_n^{\text{ET-D}} & S_n^{\text{ET-D}} & \mathbf{0} \\ \mathbf{0} & \mathbf{0} & S_n^{\text{CE-40km}} \end{bmatrix}, \end{aligned} \quad (14)$$

where $\alpha_{jk} = \alpha \delta_{jk} H(10 \text{ Hz} - k\Delta f)$, with $H(x)$ being the Heaviside step function. Given the current uncertainties surrounding the level of noise correlation, we have chosen to simulate a range of correlation coefficients, α , from 0 to 0.9 in increments of 0.1. Recent measurement using seismometers at different sites and separations showed that the coherence can range between ~ 0.01 and ~ 0.5 at the 90th percentile [13]. The coherence cannot be trivially mapped to α since it depends on the exact detector layout. Nevertheless, it gives us a rough estimate of α in the range between ~ 0.005 and ~ 0.25 , which is estimated by dividing the coherence by 2 assuming only the end test mass is subject to noise correlation.

A catalog of 200 aligned spin binary black hole merger transients using the waveform approximant IMRPhenomXPHM [28] is generated. The simulated catalog's source parameter distributions are outlined in Table I. Subsequently, we perform FIM analyses on this catalog under two different setups.

Our comparative analysis focuses on evaluating the standard deviation of individual source parameters and

the spread of the posterior distributions between the two configurations under the two scenarios. It is essential to note that the FIM only approximates the posterior primarily for high SNR signals. Thus, we set a fiducial SNR cutoff, ensuring signals possess an SNR above 50. The SNR for this cutoff is determined by the noncollocated configuration.

B. Results

Our findings reveal an improvement in measurement precision of the parameters for the vast majority of the injections when comparing the hypothetical collocated-correlated configuration with the noncollocated configuration.

In Fig. 1, we present a comparison of the performance variations between collocated and noncollocated European detector configurations as influenced by the correlation coefficient of detector noise. We show the results of the chirp mass as an example of the intrinsic parameters and the 90% credible area of sky localization as an example of the extrinsic parameters. In the left panel, we observe a decline in the ratio of the standard deviations for the chirp mass \mathcal{M}_c as the correlation coefficient increases. This trend is consistent across both EU-only and EU-US detector networks, implying an improvement in the precision of parameter estimation with greater noise correlation. The right panel presents the variation of the ratio of the 90% credible area for sky localization. Here, the sole EU network exhibits poorer performance in the collocated configuration compared to the noncollocated configuration, as anticipated due to detector separation in the noncollocated case. Remarkably, the inclusion of a US detector markedly improves performance, with the ratio nearing 1 and further reducing to 0.9 as the noise correlation reaches 0.9. This showcases that the improvement from the intrinsic parameters outweighs the additional information gained from an inter-European baseline for sky localization when an intercontinental baseline is present. The distribution of the ratio for other parameters follows the same trend and is presented in Appendix B.

To summarize the results of the FIM analysis, Table II presents the median and the 1σ interval of the ratio of posterior distributions' spreads $\hat{r}_{\text{uncorr}}^{\text{corr}}$ in the extreme scenario when the noise is highly correlated ($\alpha = 0.9$). For both cases, the $\hat{r}_{\text{uncorr}}^{\text{corr}}$ for intrinsic parameters are consistently lower than 1, signifying an improvement in parameter estimation precision. In the absence of the US detector, the $\hat{r}_{\text{uncorr}}^{\text{corr}}$ for extrinsic parameters is larger than 1. However, with a broader network with the US detector, a marked reduction below 1 suggests improved precision in extrinsic parameters with the collocated configuration in a global detector network.

Our results highlight the significant, yet positive, impact of noise correlation on parameter estimation accuracy within specific collocated GW detector configura-

TABLE I. Distribution of the source parameters in the simulation. The definition of the parameters can be referred to Ref. [29]. Cosmology from Ref. [30] is used for the luminosity distance d_L prior.

| Parameter | Distribution | Range |
|----------------------------------|-------------------------|----------------------------|
| Primary mass m_1 | Uniform | $(5, 100) M_\odot$ |
| Secondary mass m_2 | Uniform | $(5, 100) M_\odot$ |
| Primary aligned spin χ_1 | Uniform | $(0, 0.99)$ |
| Secondary aligned spin χ_2 | Uniform | $(0, 0.99)$ |
| Inclination θ_{JN} | Sine | $(0, \pi)$ |
| Polarization angle ψ | Uniform | $(0, \pi)$ |
| Right ascension α | Uniform | $(0, 2\pi)$ |
| Declination δ | Cosine | $(-\pi/2, \pi/2)$ |
| Luminosity distance d_L | Uniform in source frame | $(100, 10000) \text{ Mpc}$ |

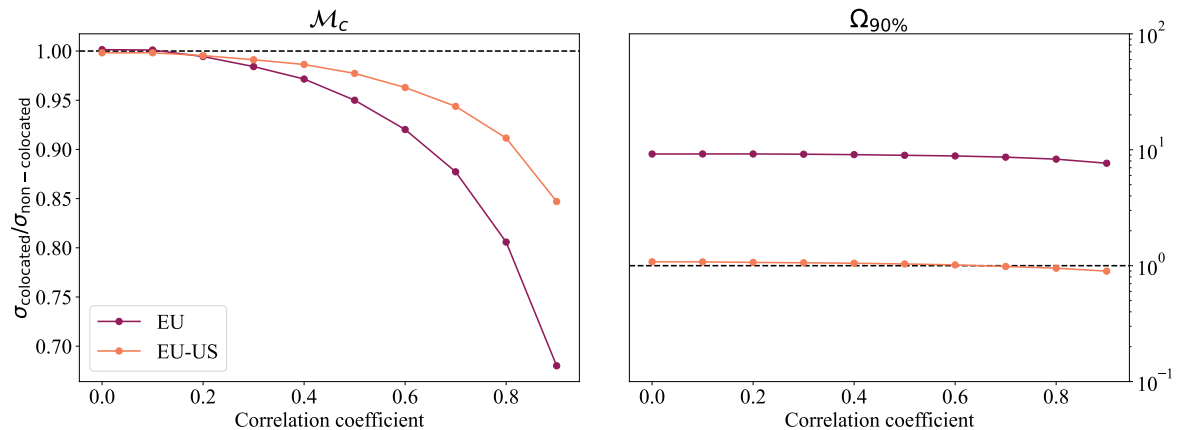


FIG. 1. This figure illustrates the variation in the medium of the ratio of the standard deviations of parameters between collocated and noncollocated EU detector configurations as the correlation coefficient of detector noise increases. The figure on the left displays the changes in the ratio for the chirp mass \mathcal{M}_c . In both the EU-only and EU-US detector networks, the ratio decreases with an increasing correlation coefficient, suggesting enhanced precision in parameter estimation. The right panel presents the variation in the ratio of the 90% credible area for sky localization. For the EU network alone, the collocated configuration underperforms relative to the noncollocated configuration. However, with the integration of a US detector, the ratio approaches 1 and further declines to 0.9 as the noise correlation increases to 0.9, indicating improved localization accuracy with higher noise correlation.

tions. This reveals the nontrivial impacts of noise correlation on the precision of parameter estimation. This underscores the important need to consider noise correlation in the design of future GW observatories, revealing its potential to improve detection capabilities.

V. CONCLUDING REMARKS

Based on the statistical foundation presented in Cireddu *et al.* [20], this work represents an initial endeavor to integrate the effects of correlated noise into the analysis of various detector designs' performance. We compared the precision of parameter estimation between a hypothetical collocated two L-shaped, correlated detector with different levels of noise correlation with a noncollocated, uncorrelated one. Our findings reveal a marked discrepancy in detector performance upon accounting for correlated noise impacts. Specifically, within the considered col-

located detector configuration, rather than a hindrance, the presence of correlated noise actually boosts our ability to extract science.

For an EU-US network setting in the highly correlated ($\alpha \approx 0.9$) scenario, the collocated-correlated detectors offers a 10%–20% improvement across parameters and an $\sim 10\%$ improvement for the sky localization, as compared to the noncollocated detectors.

A similar study comparing different detector configurations was done in Ref. [7]. Our results and Ref. [7], although partially consistent, cannot be compared directly with each other because of the different configurations considered. However, our investigations affirm that noise correlation significantly influences detector design optimization, potentially altering both quantitative and qualitative outcomes.

Our primary goal is to demonstrate that the impact of noise correlation on parameter estimation is not always negative. It is, therefore, premature to use the zero-

TABLE II. Median and 1σ uncertainty range of $\hat{r}_{\text{uncorr}}^{\text{corr}}$, assessed across all, intrinsic-only, and extrinsic-only parameters comparing the collocated configuration with a correlation coefficient of 0.9 and the noncollocated configuration. $\hat{r}_{\text{uncorr}}^{\text{corr}} < 1$ is indicating an improvement in parameter estimation precision, and vice versa. Notably, the median values for intrinsic parameters consistently remain below 1, indicating increased measurement precision. In the absence of a US detector, the $\hat{r}_{\text{uncorr}}^{\text{corr}}$ values for extrinsic parameters surpass 1. However, with a broader network with a US detector, a marked reduction below 1 suggests superior localization precision with collocated EU detectors in a global detector network.

| | EU-only network | EU-US network |
|-----------------------------------------------------|-------------------------|------------------------|
| $\hat{r}_{\text{uncorr}}^{\text{corr}}$ (all) | $0.75^{+19.72}_{-0.66}$ | $0.20^{+0.13}_{-0.06}$ |
| $\hat{r}_{\text{uncorr}}^{\text{corr}}$ (intrinsic) | $0.38^{+0.41}_{-0.17}$ | $0.65^{+0.18}_{-0.10}$ |
| $\hat{r}_{\text{uncorr}}^{\text{corr}}$ (extrinsic) | $1.50^{+44.17}_{-1.26}$ | $0.29^{+0.10}_{-0.07}$ |

correlation scenario as the upper bound for performance in correlated scenarios to simplify the analysis.

In conclusion, despite its importance, the influence of correlated noise remains overlooked in current discussions on future GW detector design. We recommend a thorough consideration of noise correlation in future research endeavors, emphasizing its potential to reshape our understanding and approach to detector design optimization in the pursuit of advancing GW astronomy.

ACKNOWLEDGEMENT

We thank Rico K. L. Lo for insightful discussions. This work was partially supported by the Research Foundation - Flanders (Grant No. I002123N). P. T. H. P is supported by the research program of the Netherlands Organization for Scientific Research (NWO). M.W. is supported by the Research Foundation - Flanders (FWO) through Grant No. 11POK24N.

SOFTWARE

The analysis and simulations presented in this work were conducted using a combination of established software

packages and custom scripts. The figures are produced using MATPLOTLIB [31, 32] and SEABORN [33]. Numerical operations and array manipulations are performed using NUMPY [34] and SCIPY [35]. To evaluate the Fisher information matrix, GWBENCH[36] is used with extension to analyze scenarios involving correlated noise.

DATA AVAILABILITY

The data generated for this publication is available on Zenodo at Ref. [37]. The postprocessing scripts used to analyze and visualize the results are archived with Zenodo at Ref. [38]. The scripts used to generate the data are not publicly available, but we are happy to share them upon request. Please note that they may require additional cleaning and documentation.

Appendix A: Determinant of the Inverse Fisher Information Matrix

The FIM is defined as

$$\mathcal{I}_{jk}(\boldsymbol{\theta}) = \mathbb{E}_{\mathbf{d}|\boldsymbol{\theta}} [(\partial_{\theta_j} \log p(\mathbf{d}|\boldsymbol{\theta}))(\partial_{\theta_k} \log p(\mathbf{d}|\boldsymbol{\theta}))] . \quad (\text{A1})$$

With the time domain likelihood function defined in Ref. [20], one can show that

$$\mathcal{I}(\boldsymbol{\theta}) = (\nabla \mathbf{s}(\boldsymbol{\theta}))^T \boldsymbol{\Sigma}_n^{-1} \nabla \mathbf{s}(\boldsymbol{\theta}) \quad (\text{A2})$$

where $\nabla \mathbf{s}(\boldsymbol{\theta})$ is the Jacobian matrix of $\mathbf{s}(\boldsymbol{\theta})$ and $\boldsymbol{\Sigma}_n$ is the noise covariance matrix. Perform a singular value decomposition on $\nabla \mathbf{s}(\boldsymbol{\theta})$, we have

$$\nabla \mathbf{s}(\boldsymbol{\theta}) = \mathbf{U}(\boldsymbol{\theta}) \mathbf{S}(\boldsymbol{\theta}) (\mathbf{V}(\boldsymbol{\theta}))^T \quad (\text{A3})$$

where $\mathbf{U}(\boldsymbol{\theta}) \in \mathbb{R}^{MN \times MN}$ and $\mathbf{V}(\boldsymbol{\theta}) \in \mathbb{R}^{D \times D}$ are orthogonal matrices, and $\mathbf{S}(\boldsymbol{\theta}) \in \mathbb{R}^{MN \times D}$ is a rectangular matrix with the singular values in the principal diagonal. M is the number of detectors, N is the number of time bins, and D is the dimensionality of the parameter space $\boldsymbol{\theta}$. Substitute the decomposition into $\hat{r}_{\text{uncorr}}^{\text{corr}}$ defined in Eq. (12), we have

$$(\hat{r}_{\text{uncorr}}^{\text{corr}})^2 \quad (\text{A4})$$

$$= \frac{\det((\nabla_{\theta} \mathbf{s}(\theta))^T (\Sigma_n^{\text{uncorr}})^{-1} (\nabla_{\theta} \mathbf{s}(\theta)))}{\det((\nabla_{\theta} \mathbf{s}(\theta))^T (\Sigma_n^{\text{corr}})^{-1} (\nabla_{\theta} \mathbf{s}(\theta)))} \Big|_{\theta=\theta_{\text{true}}} \quad (\text{A5})$$

$$= \frac{\det(\mathbf{V}(\theta) \mathbf{S}(\theta)^T \mathbf{U}(\theta)^T (\Sigma_n^{\text{uncorr}})^{-1} \mathbf{U}(\theta) \mathbf{S}(\theta) \mathbf{V}(\theta)^T)}{\det(\mathbf{V}(\theta) \mathbf{S}(\theta)^T \mathbf{U}(\theta)^T (\Sigma_n^{\text{corr}})^{-1} \mathbf{U}(\theta) \mathbf{S}(\theta) \mathbf{V}(\theta)^T)} \Big|_{\theta=\theta_{\text{true}}} \quad (\text{A6})$$

$$= \frac{(\det \mathbf{V}(\theta))^2 \det(\mathbf{S}(\theta)^T \mathbf{U}(\theta)^T (\Sigma_n^{\text{uncorr}})^{-1} \mathbf{U}(\theta) \mathbf{S}(\theta))}{(\det \mathbf{V}(\theta))^2 \det(\mathbf{S}(\theta)^T \mathbf{U}(\theta)^T (\Sigma_n^{\text{corr}})^{-1} \mathbf{U}(\theta) \mathbf{S}(\theta))} \Big|_{\theta=\theta_{\text{true}}} \quad (\text{A7})$$

$$= \frac{\det(\hat{\mathbf{S}}(\theta)^T [\mathbf{U}(\theta)^T (\Sigma_n^{\text{uncorr}})^{-1} \mathbf{U}(\theta)]_{\alpha, \alpha} \hat{\mathbf{S}}(\theta))}{\det(\hat{\mathbf{S}}(\theta)^T [\mathbf{U}(\theta)^T (\Sigma_n^{\text{corr}})^{-1} \mathbf{U}(\theta)]_{\alpha, \alpha} \hat{\mathbf{S}}(\theta))} \Big|_{\theta=\theta_{\text{true}}} \quad (\text{A8})$$

$$= \frac{(\det \hat{\mathbf{S}}(\theta))^2 \det([U(\theta)^T (\Sigma_n^{\text{uncorr}})^{-1} U(\theta)]_{\alpha, \alpha})}{(\det \hat{\mathbf{S}}(\theta))^2 \det([U(\theta)^T (\Sigma_n^{\text{corr}})^{-1} U(\theta)]_{\alpha, \alpha})} \Big|_{\theta=\theta_{\text{true}}} \quad (\text{A9})$$

$$= \frac{\det([U(\theta)^T (\Sigma_n^{\text{uncorr}})^{-1} U(\theta)]_{\alpha, \alpha})}{\det([U(\theta)^T (\Sigma_n^{\text{corr}})^{-1} U(\theta)]_{\alpha, \alpha})} \Big|_{\theta=\theta_{\text{true}}} \quad (\text{A10})$$

$$= \frac{1/\det([U(\theta)^T (\Sigma_n^{\text{corr}})^{-1} U(\theta)]_{\alpha, \alpha})}{1/\det([U(\theta)^T (\Sigma_n^{\text{uncorr}})^{-1} U(\theta)]_{\alpha, \alpha})} \Big|_{\theta=\theta_{\text{true}}} \quad (\text{A11})$$

where $\alpha = \{1, 2, \dots, D\}$ denotes the index set, and $[\cdot]_{\alpha, \alpha}$ represents the submatrix with the index set α . It is noteworthy that the spread of the posterior covariance matrix is inversely proportional

to $\sqrt{\det([U(\theta)^T (\Sigma_n^{\text{corr/uncorr}})^{-1} U(\theta)]_{\alpha, \alpha})}$. From

Eq. (A7) to Eq. (A8), we replace $\mathbf{S}(\theta)$ with $\hat{\mathbf{S}}(\theta)$ defined as a square matrix with the singular values as the diagonal entries.

The geometrical interpretation is clear: the uncertainty in parameter estimation is inversely proportional to the spread of the subspace spanned by the D principal vectors in the inverse noise covariance matrix. These vectors represent the directions in which the signal varies the most. A larger subspace spread corresponds to reduced uncertainty in estimating the model parameters.

In Eq. (A11), one shall notice that the singular values are canceled, implying that the ratio is independent of the strength of the signal. Moreover, the uncertainty is determined by the subspace spanned by the signal gradient vectors. Provided that the subspaces \mathbf{U} are the same in the numerator and the denominator, the ratio of the uncertainty is largely dependent on the spread of the noise covariance matrix. Thus, Eq. (A11) suggests that the reduced spread of the noise distribution is likely to lead to a smaller uncertainty in parameter estimation of

GW transients.

Appendix B: Distribution of the ratio of the standard deviations of all parameters

In Figure 2, we present the distributions of the ratio of the standard deviations of the individual parameters comparing the colocated configuration with different correlation coefficients and the non-colocated configuration. The left-hand side of the violin plots showcases outcomes from Europe-only network, while the right-hand side illustrates findings from an Europe-US network.

In the Europe-only network, as the correlation coefficient increases, the measurement uncertainty of the intrinsic parameters decreases. In particular, when the noise is highly correlated ($\alpha = 0.9$), the uncertainty of chirp mass \mathcal{M}_c decreases by $\sim 30\%$, with a $\sim 10\%$ decrease for the symmetric mass ratio η and the component aligned spins $\chi_{1z, 2z}$. For the extrinsic parameters, as expected, the non-colocated network is offering better estimation. Yet, it would be more realistic to consider a global detector network.

With the inclusion of the US detector at Hanford, as shown on the right-hand side of the plots, the colocated configuration improves the measurement precision of all parameters compared to the non-colocated configuration.

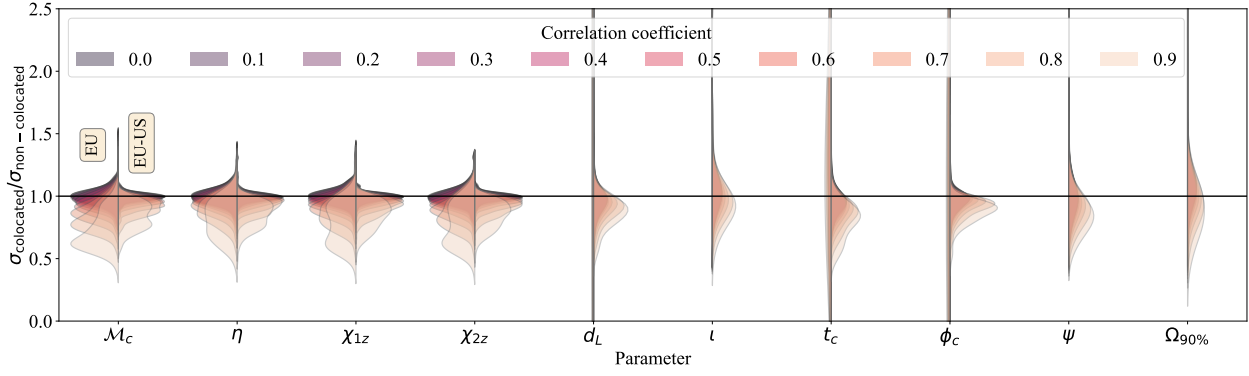


FIG. 2. The distribution of the ratio of the standard deviations of the individual parameters of the posterior distributions, with different correlation coefficients, including the chirp mass \mathcal{M}_c , symmetric mass ratio η , aligned spins $\chi_{1,2z}$, coalescence phase ϕ_c , coalescence time t_c , polarization angle ψ , inclination angle ι , and luminosity distance d_L , comparing the colocated configuration and the non-colocated configuration of the EU detectors. LHS of the plots presents the results without including the US detector. RHS of the plots presents the results including the US detector. The ratio of the 90% credible area of the sky localization $\Omega_{90\%}$ is presented in the last column.

The degree of improvement increases with the correlation coefficient. Notably, when the noise is highly correlated ($\alpha = 0.9$), the uncertainties for most of the parameters decrease by $\sim 10 - 20\%$, and the area of the 90% credible interval of the sky location $\Omega_{90\%}$ decreases by $\sim 50\%$. In Table III and Table IV, the median and 1σ intervals of the same distributions in the highly correlated scenario ($\alpha = 0.9$) are shown.

TABLE III. The median and the 1σ interval of the ratio of the standard deviations of the individual parameters in different detector networks compared to the non-colocated configuration, without the presence of the US detector. The colocated-uncorrelated EU network acts as a control to compare with colocated-correlated EU network with a correlation coefficient α of 0.9 to examine the impact of the presence of correlated noise.

[illegible]

TABLE IV. The median and the 1σ interval of the ratio of the standard deviations of the individual parameters in different detector networks compared to the non-colocated configuration, with the presence of the US detector. The colocated-uncorrelated EU network acts as a control to compare with colocated-correlated EU network with a correlation coefficient α of 0.9 to examine the impact of the presence of correlated noise.

[illegible]

-
- [1] LIGO Scientific, Virgo, B. P. Abbott *et al.*, Phys. Rev. Lett. **116**, 061102 (2016), 1602.03837.
- [2] KAGRA, VIRGO, LIGO Scientific, R. Abbott *et al.*, Phys. Rev. X **13**, 041039 (2023), 2111.03606.
- [3] LIGO Scientific, VIRGO, KAGRA, R. Abbott *et al.*, (2021), 2112.06861.
- [4] KAGRA, VIRGO, LIGO Scientific, R. Abbott *et al.*, Phys. Rev. X **13**, 011048 (2023), 2111.03634.
- [5] LIGO Scientific, VIRGO, KAGRA, R. Abbott *et al.*, (2023), 2304.08393.
- [6] M. Maggiore *et al.*, Journal of Cosmology and Astroparticle Physics **2020** (2019), arXiv: 1912.02622v4 Publisher: Institute of Physics Publishing.
- [7] M. Branchesi *et al.*, Journal of Cosmology and Astroparticle Physics **2023**, 068 (2023).
- [8] M. Evans *et al.*, A horizon study for cosmic explorer: Science, observatories, and community, 2021, 2109.09882.
- [9] P. Amaro-Seoane *et al.*, Living Reviews in Relativity **26** (2023).
- [10] M. Punturo *et al.*, Classical and Quantum Gravity **27**, 084007 (2010), Publisher: IOP Publishing.
- [11] ET steering committee, ET Design Report Update 2020, 2020.
- [12] K. Janssens, G. Boileau, N. Christensen, F. Badaracco, and N. van Remortel, Physical Review D **106**, 042008 (2022), arXiv:2206.06809 [astro-ph, physics:gr-qc].
- [13] K. Janssens *et al.*, Correlated 0.01Hz-40Hz seismic and Newtonian noise and its impact on future gravitational-wave detectors, 2024, arXiv:2402.17320 [astro-ph, physics:gr-qc, physics:physics].
- [14] K. Janssens *et al.*, Physical Review D **107**, 022004 (2023), arXiv:2209.00284 [gr-qc, physics:physics].
- [15] K. Janssens, K. Martinovic, N. Christensen, P. M. Meyers, and M. Sakellariadou, Physical Review D **104**, 122006 (2021), arXiv:2110.14730 [gr-qc].
- [16] J. Veitch *et al.*, Physical Review D **91**, 042003 (2015), arXiv:1409.7215 [astro-ph, physics:gr-qc].
- [17] G. Ashton *et al.*, The Astrophysical Journal Supplement Series **241**, 27 (2019), Publisher: The American Astronomical Society.
- [18] C. Cutler, Phys. Rev. D **57**, 7089 (1998), gr-qc/9703068.
- [19] T. A. Prince, M. Tinto, S. L. Larson, and J. W. Armstrong, Phys. Rev. D **66**, 122002 (2002), gr-qc/0209039.
- [20] F. Cireddu *et al.*, Likelihood for a network of gravitational-wave detectors with correlated noise, 2023, 2312.14614.
- [21] R. A. Horn and C. R. Johnson, *Matrix Analysis*, Repr., with corrections. ed. (Cambridge University Press, 1987).
- [22] M. Vallisneri, Physical Review D **77**, 042001 (2008), arXiv:gr-qc/0703086.
- [23] S. Hild *et al.*, Classical and Quantum Gravity **28**, 094013 (2011).
- [24] A. Puecher, A. Samajdar, and T. Dietrich, Phys. Rev. D **108**, 023018 (2023), 2304.05349.
- [25] V. Srivastava *et al.*, Astrophys. J. **931**, 22 (2022), 2201.10668.
- [26] M. Evans *et al.*, A horizon study for cosmic explorer: Science, observatories, and community, 2021, 2109.09882.
- [27] K. Kuns *et al.*, Cosmic Explorer Strain Sensitivity.
- [28] G. Pratten *et al.*, Physical Review D **103**, 104056 (2021), arXiv:2004.06503 [gr-qc].
- [29] I. M. Romero-Shaw *et al.*, Monthly Notices of the Royal Astronomical Society **499**, 3295 (2020), arXiv:2006.00714 [astro-ph, physics:gr-qc].
- [30] Planck, P. A. R. Ade *et al.*, Astron. Astrophys. **594**, A13 (2016), 1502.01589.
- [31] J. D. Hunter, Computing in Science & Engineering **9**, 90 (2007), Conference Name: Computing in Science & Engineering.
- [32] T. M. D. Team, Matplotlib: Visualization with Python, 2023, <https://doi.org/10.5281/zenodo.10150955>.
- [33] M. L. Waskom, Journal of Open Source Software **6**, 3021 (2021).
- [34] C. R. Harris *et al.*, Nature **585**, 357 (2020), Number: 7825 Publisher: Nature Publishing Group.
- [35] P. Virtanen *et al.*, Nature Methods **17**, 261 (2020), Number: 3 Publisher: Nature Publishing Group.
- [36] S. Borhanian, Classical and Quantum Gravity **38**, 175014 (2021), arXiv:2010.15202 [gr-qc].
- [37] I. C. F. Wong *et al.*, Potential impact of noise correlation in next-generation gravitational wave detectors — Data release, 2025, <https://doi.org/10.5281/zenodo.14842436>.
- [38] I. C. F. Wong, isaac-cf-wong/data-of-potential-impact-of-noise-correlation-in-next-generation-gravitational-wave-detectors: v1, 2025, <https://doi.org/10.5281/zenodo.14844558>.